Accurate and Fast Synchrophasor Estimator for Distribution Networks

Lei Chen[1], Wei Zhao[1], Fuping Wang[1], Qing Wang[2], and Songling Huang[1]

[1] State Key Lab. of Power System, Department of Electrical Engineering, Tsinghua University, Beijing 100084, China;

[2] Department of Engineering, Durham University, South Road, Durham DH1 3LY, United Kingdom

E-mail: zhaowei@mail.tsinghua.edu.cn

April 2019

Abstract. In this paper, we propose a synchrophasor estimator which can meet M and P class requirements of the IEEE standard C37.118.1 simultaneously. Meanwhile, the phase error of the estimator is always smaller than 0.05 degrees, which makes it applicable in distribution networks. The errors of the interpolated dynamic discrete Fourier transform (IpD^{2}FT) due to interharmonic interferences are investigated. Then the optimal frequencies where the IpD^{2}FT has the smallest interharmonic interference are obtained. For achieving higher accuracy, the Taylor-Fourier multifrequency model-based method is used to estimate and then eliminate the interharmonic component further. Concerning response time requirements, robust thresholds for transient detection are obtained based on numerous simulations, and the Kaiser-based IpD^{2}FT is used to meet the corresponding limits. Canonical tests stated in the IEEE standard C37.118.1 and peculiar tests which could occur in distribution networks, are both carried out to verify the performances of the proposed method.

Keywords: Distribution network, frequency, phasor measurement unit, phase, synchrophasor, rate of change of frequency.

1. Introduction

Recently, more and more distributed energy resources (DERs), such as distributed photovoltaic systems and storage systems, are connected to distribution networks (DNs). As a result, the power flows in DNs become bidirectional. Additionally, the presence of power electronic devices and time-varying loads make DNs more dynamic and unprecedented [1]. These challenges require an accurate, fast and synchronized measurement system for DN monitoring, protection, and control. Therefore, phasor measurement units (PMUs) widely used in transmission networks (TNs) are also

expected to play an important role in DNs. In the following, such two kinds of PMUs are called T-PMUs (for TNs) and D-PMUs (for DNs), respectively.

As for synchrophasor measurement in TNs, the IEEE Standard C37.118.1-2011 and its amendment Standard C37.118.1-2014 (collectively called the IEEE standard in the following) divide the T-PMUs into two classes, i.e., M class for monitoring applications requiring a higher accuracy but slower response, and P class for protection applications requiring a faster response but lower accuracy [2, 3]. However, the D-PMUs are expected to achieve high accuracy and fast response simultaneously [4, 5]. On the one hand, the power quality disturbances, such as frequency deviation, harmonic distortion, and interharmonic, could occur frequently in DNs. Also, the amplitude and phase of DNs' voltage/current can have significant fluctuations. Thus, an accurate D-PMU that can mitigate these disturbances' impacts is required. Furthermore, the short power lines and small power flows in DNs make the phase difference between two voltage nodes too small [1]. As a result, the D-PMUs should have higher phase estimation accuracy than the T-PMUs. In China, the absolute phase error limit of a D-PMU is 0.05° (i.e., 0.87 mrad). On the other hand, voltage swells and sags occur frequently in DNs, which makes us also expect the D-PMUs have a fast response, thus for fast DN situation awareness and fault location applications. As a result, the D-PMUs should return synchrophasor estimates within a few cycles. Thus, the goal of this paper is to propose a new synchrophasor estimator to have high accuracy and fast response (i.e., meet M and P class requirements) simultaneously. Meanwhile, the phase error should be smaller than the above limit in all M class accuracy tests. Although one can install two different PMUs in the same place, using a merged PMU is more reliable and inexpensive [6–8].

Regarding high accuracy, many synchrophasor estimators were proposed to mitigate the impacts of different disturbances. For example, as for frequency deviation, the interpolated discrete Fourier transform (IpDFT) is a very useful tool to reduce the error caused by spectral leakage [9]. Considering oscillation, the Taylor signal model was widely used in literature (e.g., the least square (LS) and the weighted LS) to describe dynamic phasor [10, 11]. In this way, dynamic phasor derivatives (thus synchrophasor, frequency, and rate of change of frequency (ROCOF)) can be well estimated. The interpolated dynamic DFT (IpD^{2}FT) combines the above two methods to achieve high accuracy not only under frequency deviation but also under fluctuation conditions [1]. However, when the out-of-band interference is present, none of the above methods can achieve high accuracy and fast response simultaneously. The compressive sensing of Taylor-Fourier multifrequency (TFM) model can suppress out-of-band interferences by including interharmonic in the signal model [12–15]. Nevertheless, it has a large computational burden when a large number of harmonic terms are present.

In terms of phase estimation, [16] and [17] analyzed the DFT's estimation error under frequency deviation condition, and proposed two accurate phase estimators. Unlike the above two papers concentrating on steady-state conditions, [18] made progress in estimating phase under dynamic conditions. However, none of them discussed their responsiveness under step change conditions. Moreover, [19] compares

the phase estimation accuracy of several existing methods according to the IEEE standard and EN 50160: 2010 [20].

Recently, several methods have intended to meet M and P class requirements simultaneously [6–8, 21]. In [6], a hybrid P/M class PMU was designed, which can select different class estimators (P/M class) under different conditions (transient or not). By contrast, a different scheme was proposed in [7]. The two different synchrophasor estimators have good results under steady-state and dynamic conditions, respectively. They were used to obtain estimates simultaneously, and a detector was used to select proper outputs under such two different conditions. Unlike the above two methods, a single algorithm that can meet M and P class requirements simultaneously was proposed in [8]. In [21], the Hilbert transform is used for suppressing the leakage from negative image components, and the proposed method can meet M and P class requirements over two cycles data. However, none of them have considered phase estimation accuracy, especially for DN applications. Generally, the main obstacle to such a goal is the out-of-band interferences [19]. Although [8] has proposed a method to compensate interharmonic (IH) interferences, it can only eliminate the interharmonic whose magnitude is larger than 10% of the fundamental. In practice, interharmonic magnitudes can be smaller than such a threshold, and can also cause large errors.

In this paper, the optimal frequencies for discrete-time Fourier transform (DTFT) computation are selected for both low- and high-level interharmonic interference suppression, even when it is small than the threshold stated in the IEEE standard [4]. The TFM-based method is used to reduce the errors caused by high-level interharmonics further. Concerning the response time, robust transient detection thresholds are obtained after numerous simulations, and the Kaiser-based IpD^{2}FT is used to meet overshoot requirements. As a result, the proposed method can meet M and P class requirements simultaneously, and the phase errors are always smaller than the limit mentioned earlier. Also, some peculiar conditions, which could occur in DNs, are simulated to verify the performance of the proposed method. In summary, with respect to [5–8, 21], the contributions of this paper are as follows.

- Both low- and high-level of interharmonics are considered and suppressed by optimal DTFT frequency selection and TFM-based method.
- Robust thresholds is used to detect transient conditions, and the Kaiser window are first used in the IpD^{2}FT to meet the overshoot requirements.
- Higher phase measurement accuracy is achieved, even in some peculiar conditions, e.g., harmonic distortion plus frequency deviations.

2. Proposed Synchrophasor Estimator

This section introduces the proposed synchrophasor estimator. First, the classical IpD^{2}FT [1] is briefly introduced. Then, an optimal DFT frequency selection scheme is introduced for interharmonic suppression. Next, an interharmonic elimination method

is proposed to mitigate the interharmonic's impact further. Afterward, the dynamic response of the proposed method is considered. Finally, the implementation steps of the proposed method are summarized.

2.1. Introduction of the Classical IpD²FT

Generally, a dynamic signal can be modeled as

$$\begin{aligned} s(t) &= a(t)\cos(2\pi ft + \phi(t)) \\ &= \sqrt{2}\mathrm{Re}\{x(t)e^{j2\pi ft}\} \end{aligned} \tag{1}$$

where $a(t)$ and $\phi(t)$ is the dynamic amplitude and phase, respectively; f and f_0 is the actual and nominal frequency; $x(t) = (a(t)/\sqrt{2})e^{j\phi(t)}$ is the dynamic phasor; and $\mathrm{Re}\{\cdot\}$ is the operation picking the real part of the phasor. Please note that f can have a static deviation from the nominal frequency f_0, i.e., $\Delta f = f - f_0$. However, the synchrophasor $p(t)$ is a phasor referred to f_0 [2], which is given by

$$p(t) = x(t)e^{j2\pi\Delta ft} \tag{2}$$

The Taylor series expansion is used to describe the fundamental phasor $x(t)$ [10], and then (1) can be described as

$$s(t) = \sqrt{2}\mathrm{Re}\{(x_0 + tx_1 + ... + \frac{t^K}{K!}x_\mathrm{K})e^{j2\pi f_\mathrm{m}t}\} \quad -\frac{T_\mathrm{w}}{2} \le t \le \frac{T_\mathrm{w}}{2} \tag{3}$$

where x_k (with $k = 0, 1, ..., K$) is the k-th derivative of $p(t)$ at time $t = 0$; T_w is the interval length of the observation window; and f_m is the model frequency.

We assume that N_0 samples are obtained in every nominal cycle (thus the sampling frequency is $f_\mathrm{s} = N_0 f_0$). Accordingly, $N_\mathrm{w} = cN_0 - 1$ samples are obtained in the observation window $-T_\mathrm{w}/2 \le t \le T_\mathrm{w}/2$, where c is the integer nominal cycle number of the observation window. In this paper, $c = 4$ is particularly used for synchrophasor estimation. In order to make $t = 0$ at the center of the window, we let N_w be an odd number. If we compute windowed DTFT of (3), we have

$$\begin{aligned} S(f_b) &= \frac{\sqrt{2}}{N_\mathrm{w}}\sum_{n=-N}^{N} s(n)w(n)e^{-j2\pi f_b n/f_s} \\ &= \sum_{k=0}^{K}[x_k W_k(f_b - f_\mathrm{m}) + x_k^* W_k(f_b + f_\mathrm{m})] \end{aligned} \tag{4}$$

where $N = (N_\mathrm{w} - 1)/2$; * is the operator returning the conjugate phasor; and

$$W_k(f_b) = \frac{1}{N_\mathrm{w}}\sum_{n=-N}^{N}\frac{1}{k!}(\frac{n}{f_s})^k w(n)e^{-j2\pi f_b n/f_s} \tag{5}$$

is a function related to the Taylor expansion order k.

Typically, the Taylor series is truncated to the second order, i.e., $K = 2$ [1]. In this paper, we compute the windowed DTFT of (3) (after being sampled) at three different frequencies f_b (with $b = 1, 2, 3$). Then we have [1]

$$\boldsymbol{S} = \boldsymbol{W}_\mathrm{r}\boldsymbol{X} + \boldsymbol{W}_\mathrm{i}\boldsymbol{X}^* \tag{6}$$

where $\boldsymbol{S}$ is a column vector consisting of $S(f_b)$ (with $b = 1, 2, 3$); $\boldsymbol{W}_{\mathrm{r}}$ is a matrix consisting of $W_k(f_b - f_{\mathrm{m}})$ (with $k = 0, 1, 2,\ b = 1, 2, 3$); $\boldsymbol{W}_{\mathrm{i}}$ is a matrix consisting of $W_k(f_b + f_{\mathrm{m}})$ (with $k = 0, 1, 2,\ b = 1, 2, 3$); and $\boldsymbol{X}$ is a column vector consisting of x_0, x_1 and x_2. In the classical IpD^{2}FT, the bin frequencies $\{(c-1)f_{\mathrm{s}}/N_{\mathrm{w}}, cf_{\mathrm{s}}/N_{\mathrm{w}}, (c+1)f_{\mathrm{s}}/N_{\mathrm{w}}\}$ are selected as f_b (with $b = 1, 2, 3$).

By using the matrix inversion method to solve (6) [5], we can obtain the fundamental phasor derivative estimates $\hat{x}_k$ (with $k = 0, 1, 2$). Then the synchrophasor estimates can be obtained according to (2). Additionally, according to [10], the fundamental phase, frequency, ROCOF and the first-order derivative of the amplitude can be estimated by

$$\hat{\phi} = \mathrm{atan}\frac{\mathrm{Re}\{\hat{x}_0\}}{\mathrm{Im}\{\hat{x}_0\}} \tag{7}$$

$$\hat{f} = f_{\mathrm{m}} + \frac{1}{2\pi}\frac{\mathrm{Im}\{\hat{x}_1\hat{x}_0^*\}}{|\hat{x}_0|^2} \tag{8}$$

$$\widehat{ROCOF} = \frac{1}{\pi}\frac{\mathrm{Im}\{\hat{x}_2\hat{x}_0^*\}}{|\hat{x}_0|^2} - \frac{1}{\pi}\frac{\mathrm{Re}\{\hat{x}_1\hat{x}_0^*\}\mathrm{Im}\{\hat{x}_1\hat{x}_0^*\}}{|\hat{x}_0|^4} \tag{9}$$

$$\hat{a}' = \sqrt{2}\mathrm{Re}\{\hat{x}_1 e^{-j\hat{\phi}}\} \tag{10}$$

where $\mathrm{Im}\{\cdot\}$ is the operation picking the imaginary part of the phasor; and $\hat{}$ represents the corresponding value is the estimated one. Generally, any window function can be used in this method. In this paper, we use the Hanning window and Kaiser window in steady-state and dynamic conditions, respectively. A first frequency estimation is carried out based on the Hanning-based three-point IpDFT [22] (called the IpDFT in the following for simplicity) for determining the model frequency f_{m}. More details about such a method can be found in [23].

2.2. DTFT Frequency Selection for Interharmonic Suppression

One of the main uncertainty contributions of the IpD^{2}FT is the interharmonic interference. This section discusses the DTFT frequency selection scheme for interharmonic interference suppression.

According to [2], a single interharmonic with frequency f_{ih} within $[10, 50 - RR/2]$ or $[100 - RR/2, 100)$ Hz should be included in the signal model (1) to test a synchrophasor estimator, where RR is the reporting rate of a PMU. Generally, a discrete interharmonic component can be defined as

$$s_{\mathrm{ih}}[n] = a_{\mathrm{ih}}\cos(2\pi f_{\mathrm{ih}}\frac{n}{f_{\mathrm{s}}} + \phi_{\mathrm{ih}}) \tag{11}$$

where a_{ih}, f_{ih}, and ϕ_{ih} are the interharmonic amplitude, frequency, and phase, respectively. After some deductions, the DTFT of (11) with adopting the Hanning

window is as follows [4, 24]

$$\begin{aligned} S_{\rm ih}(f_b) &= \frac{a_{\rm ih}e^{j\varphi_{\rm ih}}}{4N_{\rm w}}\sum_{m=0}^{1}\sum_{n=-N}^{N}\frac{e^{-j\frac{2\pi n}{f_s}[(f_b-f_{\rm ih})-m\frac{f_s}{N_{\rm w}}]}+e^{-j\frac{2\pi n}{f_s}[(f_b-f_{\rm ih})+m\frac{f_s}{N_{\rm w}}]}}{2} \\ &+ \frac{a_{\rm ih}e^{-j\varphi_{\rm ih}}}{4N_{\rm w}}\sum_{m=0}^{1}\sum_{n=-N}^{N}\frac{e^{-j\frac{2\pi n}{f_s}[(f_b+f_{\rm ih})-m\frac{f_s}{N_{\rm w}}]}+e^{-j\frac{2\pi n}{f_s}[(f_b+f_{\rm ih})+m\frac{f_s}{N_{\rm w}}]}}{2} \\ &= \frac{1}{2}a_{\rm ih}e^{j\phi_{\rm ih}}\cdot D(f_b-f_{\rm ih})\cdot R(f_b-f_{\rm ih}) \\ &+ \frac{1}{2}a_{\rm ih}e^{-j\phi_{\rm ih}}\cdot D(f_b+f_{\rm ih})\cdot R(f_b+f_{\rm ih}) \end{aligned} \tag{12}$$

where

$$D(f) = \frac{\sin(\frac{\pi N_{\rm w}f}{f_{\rm s}})}{N_{\rm w}\sin(\frac{\pi f}{f_{\rm s}})} \tag{13}$$

corresponds to the Dirichlet kernel related to the rectangular window; and

$$R(f) = \frac{1}{2} - \frac{1}{2}\cdot\frac{\sin^2(\frac{\pi f}{f_{\rm s}})\cdot\cos(\frac{\pi}{N_{\rm w}})}{\sin^2(\frac{\pi f}{f_{\rm s}})-\sin^2(\frac{\pi}{N_{\rm w}})} \tag{14}$$

is a continuous function related to the Hanning window. When an interharmonic component exists, $S_{\rm ih}(f_b)$ will be added to the elements of vector $\boldsymbol{S}$, and errors arise. As seen, $S_{\rm ih}(f_b)$ has two components, i.e., the positive interharmonic component [the former term of (12)] and negative interharmonic component [the latter term of (12)].

If the sampling frequency is high enough (e.g., $f_{\rm s} > 5$ kHz), we have $\sin^2(\pi f/f_{\rm s}) \approx \pi f/f_{\rm s}$, $\cos(\pi/N_{\rm w}) \approx 1$, and $\sin^2(\pi/N_{\rm w}) \approx \pi/N_{\rm w}$ [24], and then

$$R(f) \approx \frac{1}{2} - \frac{1}{2}\cdot\frac{(\frac{\pi f}{f_{\rm s}})^2}{(\frac{\pi f}{f_{\rm s}})^2-(\frac{\pi}{N_{\rm w}})^2} \tag{15}$$

Typically, RR is selected as 50 frames/s. Thus, $f_{\rm ih}$ is within $[10, 25]$ or $[75, 100)$ Hz. If the bin frequencies $\{3f_{\rm s}/N_{\rm w}, 4f_{\rm s}/N_{\rm w}, 5f_{\rm s}/N_{\rm w}\}$ are selected as f_b, we have $(\pi(f_b+f_{\rm ih})/f_{\rm s})^2 \gg (\pi/N_{\rm w})^2$, and then

$$R(f_b+f_{\rm ih}) \approx 0 \tag{16}$$

Thus, the negative interharmonic component has few leakages on the DTFT values computed at bin frequencies. However, because the bin frequencies may be close to the interharmonic frequency, $(\pi(f_b-f_{\rm ih})/f_{\rm s})^2$ and $(\pi/N_{\rm w})^2$ could have small difference. As a result, the positive interharmonic component will cause large interferences.

Let us first consider the condition of $f_{\rm ih} \in [10, 25]$ Hz. If we select $\{f_{\rm ih}+2f_{\rm s}/N_{\rm w}, f_{\rm ih}+3f_{\rm s}/N_{\rm w}, f_{\rm ih}+4f_{\rm s}/N_{\rm w}\}$ as f_b, we can obtain $D(f_b-f_{\rm ih}) = 0$ and $R(f_b+f_{\rm ih}) \approx 0$, and then $S_{\rm ih}(f_b) \approx 0$. In this way, the interharmonic interference will be almost null. Thus, we can easily obtain the optimal DTFT frequencies for $f_{\rm ih} \in [10, 25]$ Hz are $\{f_{\rm ih}+2f_{\rm s}/N_{\rm w}, f_{\rm ih}+3f_{\rm s}/N_{\rm w}, f_{\rm ih}+4f_{\rm s}/N_{\rm w}\}$.

Similarly, when $f_{\rm ih} \in [75, 100)$ Hz, the optimal DTFT frequencies are $\{f_{\rm ih}-2f_{\rm s}/N_{\rm w}, f_{\rm ih}-3f_{\rm s}/N_{\rm w}, f_{\rm ih}-4f_{\rm s}/N_{\rm w}\}$. However, when there is no interharmonic component, the bin frequencies are still used for the DTFT computation.

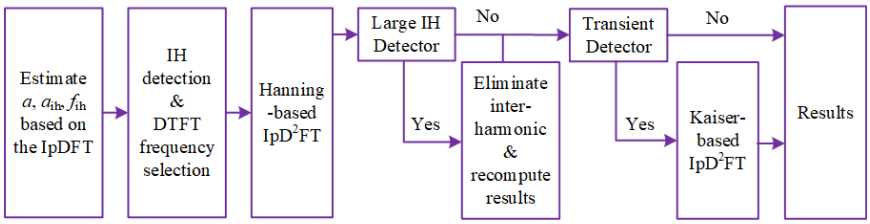

Figure 1. Implementation steps of the proposed method. IH detection and DTFT frequency selection are carried out according to (19). Large IH Detector has two detection conditions, which are $5 < \hat{f}_{\text{ih}} < 27$ Hz || $73 < \hat{f}_{\text{ih}} < 101$ Hz and $\hat{a}_{\text{ih}} > 0.72\%\hat{a}$. Transient Detector has one detection condition, which is $|\widehat{ROCOF}| > 0.85$ Hz/s || $|\hat{a}'| > 0.1$ p.u./s.

Because the interharmonic frequency is practically unknown, a prior frequency estimation should be carried out. First, we use the IpDFT to obtain the fundamental parameter estimates $\{\hat{a}, \hat{\phi}, \hat{f}\}$ (see [23]). Then the fundamental signal is regenerated by using these estimates [see (17)] and removed from the original signal [see (18)]. The residual signal $r[n]$ is used to estimate the interharmonic frequency f_{ih} based on the IpDFT (see [23]).

$$\hat{s}[n] = \hat{a}\cos(2\pi\hat{f}\frac{n}{f_{\text{s}}} + \hat{\phi}) \quad (n = -N, ..., N) \tag{17}$$

$$r[n] = s[n] - \hat{s}[n] \quad (n = -N, ..., N) \tag{18}$$

When implementing the IpDFT, if the frequency of the peak bin of the residual signal is smaller than 50 Hz (i.e., the interharmonic frequency is within [10, 25] Hz), the 1st, 2nd, and 3rd bins are always selected for interpolation (see [23]). such a method is a balance between the infiltration from the negative interharmonic and positive fundamental components. Although the 2nd bin is not always the peak one, these three bins have enough information for interpolation. This part corresponds to the implementation step of fundamental and interharmonic parameters estimation (see the first step of Fig. 1).

After estimating the fundamental and interharmonic frequencies and amplitudes, we can select the DTFT frequencies with the following scheme.

$$\begin{cases} \{\hat{f}_{\text{ih}} + \frac{2f_{\text{s}}}{N_{\text{w}}}, \hat{f}_{\text{ih}} + \frac{3f_{\text{s}}}{N_{\text{w}}}, \hat{f}_{\text{ih}} + \frac{4f_{\text{s}}}{N_{\text{w}}}\}, & \hat{f}_{\text{ih}} \in (5, 27)\&\& \\ & \hat{a}_{\text{ih}} > 0.1\%\hat{a} \\ \{\hat{f}_{\text{ih}} - \frac{2f_{\text{s}}}{N_{\text{w}}}, \hat{f}_{\text{ih}} - \frac{3f_{\text{s}}}{N_{\text{w}}}, \hat{f}_{\text{ih}} - \frac{4f_{\text{s}}}{N_{\text{w}}}\}, & \hat{f}_{\text{ih}} \in (73, 101)\&\& \\ & \hat{a}_{\text{ih}} > 0.1\%\hat{a} \\ \{\frac{3f_{\text{s}}}{N_{\text{w}}}, \frac{4f_{\text{s}}}{N_{\text{w}}}, \frac{5f_{\text{s}}}{N_{\text{w}}}\}, & others \end{cases} \tag{19}$$

If the estimated interharmonic amplitude $\hat{a}_{\text{ih}}$ is smaller than $0.1\%\hat{a}$, the bin frequencies are selected for the IpD^{2}FT to estimate the fundamental parameters.

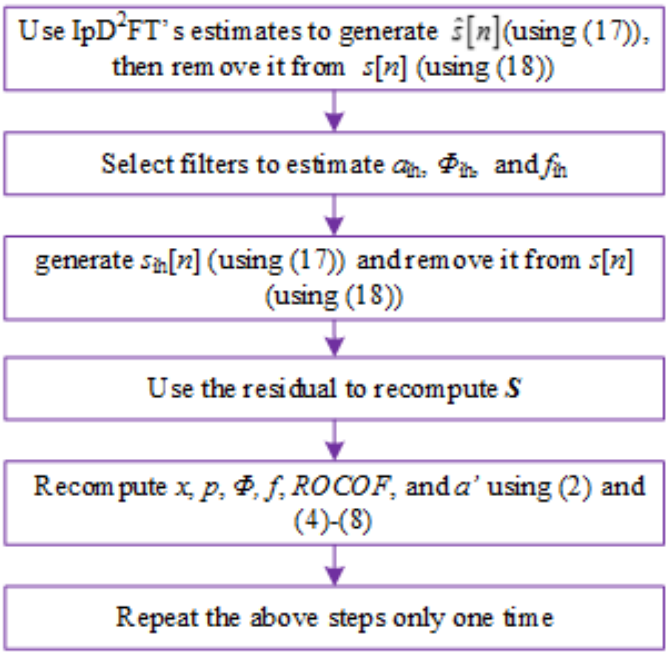

Figure 2. Illustration of interharmonic elimination and result recomputation.

Otherwise, when the estimated interharmonic frequency $\hat{f}_{\text{ih}}$ is within (5, 27) Hz or (73, 101) Hz, the optimal DTFT frequencies are selected. Please note that because f_{ih} cannot be estimated accurately, the frequency ranges are wider than the actual ones. Unlike [8], we consider the possible interharmonic component with an amplitude much smaller than 10% of the fundamental. Thus, a threshold of 0.1% is used. Although the interharmonic amplitude can be smaller than such a threshold, the errors are negligible, which can be observed in section 4.6.

2.3. Interharmonic Elimination and Result Recomputation

In the worst conditions (high ratio of an interharmonic component), the interharmonic frequency cannot be accurately estimated by the IpDFT. As a result, the requirements stated in section 1 still cannot be met. In this section, we combine the least square method and the TFM model [12] to suppress the interharmonic interference further [8].

In the TFM model, the fundamental component and a single interharmonic are both included (please see [25] for more details). The Taylor signal model is truncated to the second order. The interharmonic phasor derivatives (thus phasor and frequency) are estimated based on the least square method. Then the interharmonic can be reconstructed [similar to (17)] and eliminated from the original signal [similar to (18)] [10]. In order to reduce the computational burden, the parameter estimation filters are precalculated. The fundamental frequency is set at the nominal value f_0. The interharmonic center frequencies are within [10, 25] and [75, 100] Hz in a step of 1 Hz. At each center frequency, two filters for the zeroth- and first-derivatives estimation are stored.

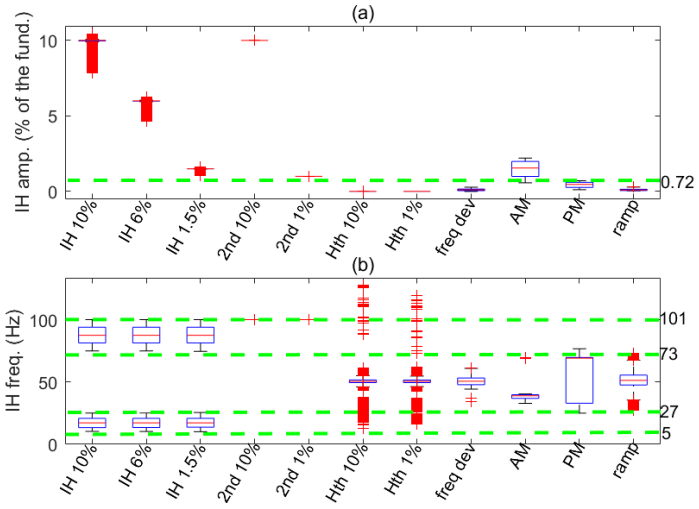

Figure 3. Boxplot of interharmonic amplitude [(a)] and frequency [(b)] estimates in the first step of Fig. 1 (SNR=80 dB). IH: interharmonic; 2nd: harmonic distortion (2nd); Hth: harmonic distortion (3rd-50th); freq dev: frequency deviation (-5∼5 Hz); AM: amplitude modulation (5 Hz); PM: phase modulation (5 Hz); ramp: frequency ramp (±1 Hz/s).

The detailed implementation steps of interharmonic elimination and result recomputation are illustrated in Fig. 2. The interharmonic frequency estimated by the IpDFT is used to select the filters with the closest interharmonic center frequency. After using the filters' estimates to reconstruct and eliminate the interharmonic from the original signal [8], the vector $\boldsymbol{S}$ is recomputed by using the residual signal. Then it is used to estimate the fundamental parameters through the IpD^{2}FT. Finally, another iteration is processed to achieve high accuracy.

In order to detect large interharmonic interferences, a detector should be used. In Fig. 3, the ranges of $\hat{a}_{\text{ih}}$ and $\hat{f}_{\text{ih}}$ after carrying out the first step of Fig. 1 are shown. Because amplitude and phase step changes will be detected and processed in the following steps, they are not included in this boxplot. Wideband Gaussian noise with the signal-to-noise ratio (SNR) equal to 80 dB is added to all the test signals. Interharmonics with different magnitudes (10%, 6%, and 1.5% of the fundamental) are included in the signal for tests. It is observed that when the two detection conditions of $5 < \hat{f}_{\text{ih}} < 27$ Hz $\|$ $73 < \hat{f}_{\text{ih}} < 101$ Hz and $\hat{a}_{\text{ih}} > 0.72\%\hat{a}$ are used, interharmonics with amplitudes equal to 1.5% of the fundamental can be completely detected. Although the 2nd harmonic can also be detected with using these two conditions, it will be eliminated by the proposed method too. Such a detector corresponds to the Large IH Detector in Fig. 1.

2.4. Dynamic Response

When the optimal DTFT frequencies (not the bin frequencies) are selected or the step of interharmonic elimination is activated, the dynamic response of the proposed method

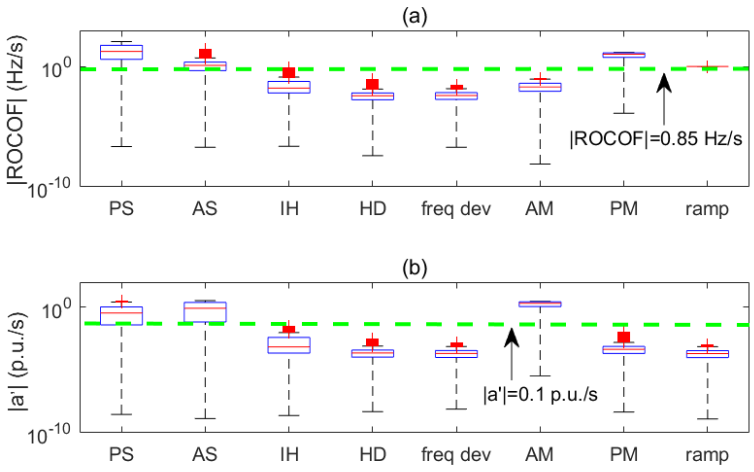

Figure 4. Boxplot of absolute ROCOF [(a)] and amplitude derivative [(b)] estimates after the first 5 steps of Fig. 1 (SNR=80 dB). PS: phase step (±0.1 rad); AS: amplitude step (±10%); IH: interharmonic (0.05% ∼10%); HD: harmonic distortion (2nd-50th, 10%); freq dev: frequency deviation (-5∼5 Hz); AM: amplitude modulation (5 Hz); PM: phase modulation (5 Hz); ramp: frequency ramp (±1 Hz/s).

could be slower. This section devotes to enhancing the dynamic response of the method. We use a detector to detect the fast changes of the amplitude or phase, and the Kaiser-based IpD^{2}FT is used to estimate fundamental parameters. Please note that because the Hanning-based IpD^{2}FT cannot meet the overshoot requirements of the IEEE standard, we use the Kaiser window to replace the Hanning window, thus for smoothing the amplitude estimates. The parameter β of the Kaiser window is set at 6. The bin frequencies are selected as the DTFT frequencies.

Concerning the Transient Detector (see Fig. 1), it is required to be robust to other disturbances, such as harmonic distortion and frequency deviation. In Fig. 4, the ranges of $|\widehat{ROCOF}|$ and $|\hat{a}'|$ after carrying out the first 5 steps of Fig. 1 are presented. As seen, when the detect condition of $|\widehat{ROCOF}| > 0.85$ Hz/s $||$ $|\hat{a}'| > 0.1$ p.u./s is used, the amplitude or phase step change condition can activate the following procedure, i.e., Kaiser-based IpD^{2}FT. Although fast amplitude and phase modulations can also activate the Kaiser-based IpD^{2}FT, the accuracy requirements can still be met. The use of two parameters for condition detection makes the proposed method more robust than the method only using one of them.

2.5. Implementation Steps

This section summarizes the implementation steps of the proposed method for details (see Fig. 1). First, parameters a, a_{ih}, and f_{ih} are estimated by the IpDFT (see [23], and then they are used to detect interharmonics and select proper DTFT frequencies according to (19).

After the DTFT frequencies are selected, the Hanning-based IpD^{2}FT is used

to obtain fundamental parameter estimates $\{\hat{x},\ \hat{p},\ \hat{\phi}, \hat{f}, \widehat{ROCOF}, \hat{a}'\}$. In order to achieve a high accuracy under large interharmonic interferences, a further interharmonic elimination should be carried out. The Large IH Detector is used to detect if there is large interharmonic interference. The detection conditions are given in the legend of Fig. 1. Please note that the interharmonic amplitude requirement in such a detector ($\hat{a}_{\rm ih} > 0.72\%\hat{a}$) is looser than that in (19) ($\hat{a}_{\rm ih} > 0.1\%\hat{a}$). This is because a fake interharmonic can be detected under frequency ramp and modulation conditions. The IEEE standard requirements cannot be met if the interharmonic elimination is activated in such conditions. The impacts of interharmonics with small amplitudes can be only mitigated based on the optimal DTFT frequency selection.

The Transient Detector uses the estimates of ROCOF and a' to detect amplitude and phase step change conditions. If the detection condition (see the legend of Fig. 1) is satisfied, the Kaiser-based IpD^{2}FT is used to estimate the fundamental parameters again. Since the proposed method is an improved version of the IpD^{2}FT, it is called the i-IpD^{2}FT synchrophasor estimator in the following.

3. Computation Time and Reporting Latency

The main computations of the i-IpD^{2}FT in each step are listed in Table 1. As seen, a large number of computations are for steps 3 and 7, i.e., implementing the IpD^{2}FT. A first fundamental frequency estimation helps to reduce the times of matrix generation. By contrast, the classical IpD^{2}FT needs several iterations to get accurate fundamental frequency estimates. As a result, many times of matrix generation ($\boldsymbol{W}_{\rm r}$ and $\boldsymbol{W}_{\rm i}$) are needed. In step 5, only the vector $\boldsymbol{S}$ is recalculated after eliminating the interharmonic from the original signal. Thus, the computation time can also be reduced.

When all the steps in the i-IpD^{2}FT are carried out, the total floating-point operations of the i-IpD^{2}FT are $261N_{\rm w} + 7516$. Thus, the computation time is determined by the sampling frequency. The higher the sampling frequency, the longer the computation time. We assume the signal is sampled at $f_{\rm s} = 8$ kHz (f_0=50 Hz). Then 174295 floating-point operations are needed ($N_{\rm w} = 639$). Texas Instruments Inc. provides a floating-point digital processor TMS320C6713BGDP300, which can execute

Table 1. Main computations of the i-IpD^{2}FT. The lower-upper decomposition-based method is used for matrix inversion.

Step	**Computation Type**	
	cos, sin, $\times$, $\div$	$+$, $-$
1	$28N_{\rm w}$	$25N_{\rm w} - 24$
3	$48N_{\rm w} + 1648$	$24N_{\rm w} + 236$
5	$40N_{\rm w} + 3296$	$24N_{\rm w} + 500$
7	$48N_{\rm w} + 1648$	$24N_{\rm w} + 236$

1800 million floating-point operations every second. If it is used in a D-PMU, the computation time will be 0.10 ms. As for a D-PMU with a reporting rate of 50 frames/s, it is much smaller than the upper bound of 20 ms.

Because the estimates are obtained at the center window, the reporting latency is half of the window length, i.e., 39.88 ms for $f_s = 8$ kHz. Consequently, the reporting latency is smaller than the limit of 40 ms (for P class PMUs).

4. Performance Evaluation

This section evaluates the i-IpD^{2}FT's performances under canonical conditions stated in the IEEE standard (including P and M class tests) and some peculiar conditions in DNs [1]. On the evaluation of the i-IpD^{2}FT's accuracy, not only the total vector error (TVE), frequency error (FE), and ROCOF error (RFE) but also the phase error (PE) (all in absolute values) are compared with the corresponding limits (RR=50 frames/s). Accordingly, the responsiveness of the i-IpD^{2}FT is evaluated in amplitude and phase step change tests. The popular IpD^{2}FT, which is proposed especially for DNs, is also simulated for comparing results with the i-IpD^{2}FT.

In order to simulate the real work conditions, wideband noise with a signal-to-noise ratio (SNR) of 80 dB is added to each test signal. The sampling frequency is set to 8 kHz. The observation window of the i-IpD^{2}FT is 4 cycles long. The maximum errors are obtained over a window with 5 s duration except for modulation and frequency ramp tests, where the duration can be up to 20 s.

4.1. Frequency Deviations

In DNs, frequency deviation is one of the power quality disturbances that may occur frequently. It is necessary to test the i-IpD^{2}FT's performances under frequency deviation conditions.

In this test, we consider that the fundamental frequency of the test signal has a deviation of ± 2 Hz (for P class test) or ± 5 Hz (for M class test). The corresponding results (all in maximum errors) and limits stated in the IEEE standard are shown in Table 2. We can see that all errors of the i-IpD^{2}FT are much smaller than the corresponding limits, even in M class tests. Particularly, the maximum phase errors in P and M class tests are only 0.03 and 0.04 mrad, respectively, which are only about 5% of the limit (0.87 mrad). This evidence shows that the i-IpD^{2}FT has a high accuracy under frequency deviation conditions, and the phase estimation accuracy is suitable for DN applications.

It is interesting that the results in P and M class tests have few differences. This is because the fundamental frequency estimation (step 1 in Fig. 1) helps to design an accurate signal model for the Hanning-based IpD^{2}FT (step 3). As a result, frequency deviation has few impacts on synchrophasor, frequency, ROCOF, and phase estimations. Because there are no interharmonics in the signal, the performances of the i-IpD^{2}FT

Table 2. Results and corresponding limits in frequency deviation Test. SNR=80 dB

Parm.	**TVE (%)**		**FE (mHz)**		**RFE (Hz/s)**		**PE (mrad)**	
Class	P	M	P	M	P	M	P	M
Std.	1	1	5	5	0.4	0.1	0.87	0.87
i-IpD^{2}FT	0.003	0.003	0.22	0.23	0.02	0.03	0.02	0.03
IpD^{2}FT	0.003	0.003	0.22	0.23	0.02	0.03	0.02	0.03

Table 3. Results and corresponding limits in harmonic distortion test. SNR=80 dB

Parm.	**TVE (%)**		**FE (mHz)**		**RFE (Hz/s)**		**PE (mrad)**	
Class	P	M	P	M	P	M	P	M
Std.	1	1	5	25	–	–	0.87	0.87
i-IpD^{2}FT	0.005	0.006	0.36	0.42	0.06	0.08	0.05	0.06
IpD^{2}FT	0.003	0.008	0.17	0.53	0.03	0.13	0.02	0.07

and IpD^{2}FT are almost the same.

4.2. Harmonic Distortions

Because more and more DERs are connected to DNs, harmonics are widely present in voltage/current signals. In this test, a single harmonic up to the 50th is added to the signal. The fundamental frequency is set to the nominal value (50 Hz). In P and M class tests, the harmonic magnitude is set to 1% and 10% of the fundamental, respectively.

The results and the corresponding limits are provided in Table 3. Compared with the results in the frequency deviation test, all the errors (TVE, FE, RFE, and PE) become larger. Therefore, harmonic distortion has a worse impact on synchrophasor estimation. However, all the errors of the i-IpD^{2}FT are much smaller than the corresponding limits. Although in the newest IEEE standard, there are no RFE limits for harmonic distortion tests [3], the maximum RFEs in the P and M class tests are only 0.05 and 0.06 Hz/s, respectively. In such a condition, the performances of the i-IpD^{2}FT and IpD^{2}FT have few differences.

4.3. Harmonic Distortions plus Frequency deviation

In DNs, harmonic distortions and large frequency deviations may be present simultaneously in a current signal [1]. We also test the proposed method in such a peculiar condition. The test signal contains 1% 2nd harmonic, 3% 3rd harmonic, 3% 5th harmonic, 2% 7th harmonic, and 1% 9th harmonic. The fundamental frequency has a deviation of ± 5 Hz, and the hth harmonic's frequency is h times of the fundamental one. The corresponding results are presented in Table 4. The estimation errors of the i-IpD^{2}FT are larger than those of the IpD^{2}FT. If the P class limits (stricter than M class requirements) in harmonic distortion test are also used in this test, the proposed

Table 4. Results under the joint impacts of harmonic distortion and frequency deviation. SNR=80 dB

Parm.	**TVE (%)**		**FE (mHz)**		**RFE (Hz/s)**		**PE (mrad)**	
Std. (P)	1		5		–		0.87	
f **(Hz)**	45	55	45	55	45	55	45	55
i-IpD^{2}FT	0.07	0.009	2.44	0.77	0.77	0.13	0.38	0.09
IpD^{2}FT	0.03	0.009	0.66	0.77	0.66	0.13	0.31	0.09

method can still meet the requirements. The proposed method is still useful in such a condition. It is observed that the errors with f =45 Hz are much larger than those with f =55 Hz. This is because when the fundamental deviation Δf is -5 Hz, the spectral leakage is larger than that with Δf=5 Hz.

4.4. Unbalance in Three-phase System

Three-phase unbalance can occur in DNs due to unbalanced loads, power lines and so on. The proposed estimator's performance should be evaluated in such a condition. First of all, the synchrophasors, frequencies, and ROCOFs of the three phases are estimated. Then, the positive sequence synchrophasor is obtained based on the Fortescue transformation. The final frequency and ROCOF estimates are obtained by averaging the three-phase results.

The test signal is shown in (20), which is referred to [26], where f is the fundamental frequency. The magnitude and phase of the signal in Phase A introduce unbalance, where the magnitude has a difference of 20% with respect to the balance one, and the phase has a difference of π rad with respect to the balance one. As known, such a degree of unbalance is very high. The fundamental frequency is set to 49.5 Hz. In Table 5, the maximum errors of the i-IpD^{2}FT and IpD^{2}FT are shown.

$$\begin{aligned} s_{\mathrm{A}}(t) &= 1.2\cos(2\pi f t + \pi) \\ s_{\mathrm{B}}(t) &= \cos(2\pi f t - \frac{2}{3}\pi) \\ s_{\mathrm{C}}(t) &= \cos(2\pi f t + \frac{2}{3}\pi) \end{aligned} \tag{20}$$

As seen, the estimation errors of the i-IpD^{2}FT in such a condition are very small. For example, the maximum PE is almost 0 rad, which shows that the proposed method can be applied to unbalance condition. Also, the results of the i-IpD^{2}FT and IpD^{2}FT are almost the same. This is because the i-IpD^{2}FT and IpD^{2}FT set almost the same fundamental frequencies in the Taylor signal model. There is no standard limits on such a condition. If the M-class limits in frequency deviation condition are also referred to in this test, the i-IpD^{2}FT can meet the requirements.

Table 5. Maximum errors under three-phase unbalance condition. SNR=80 dB, $f = 49.5$ Hz

Parm.	**TVE (%)**	**FE (mHz)**	**RFE (Hz/s)**	**PE (mrad)**
Std. (M)	1	5	0.1	0.87
i-IpD^{2}FT	0.00	0.10	0.01	0.00
IpD^{2}FT	0.00	0.10	0.01	0.00

Table 6. Maximum errors under high-level noise condition (M class requirements in harmonic distortion conditions are referred to). SNR=50 dB

Parm.	**TVE (%)**	**FE (mHz)**	**RFE (Hz/s)**	**PE (mrad)**
Std. (M)	1	5	–	0.87
i-IpD^{2}FT	0.08	4.87	0.52	0.62
IpD^{2}FT	0.08	4.87	0.52	0.62

4.5. High-level Noise

Because the DNs are close to loads, the current signal may contain high-level noise. In this section, a signal with 50-dB wideband Gaussian noise is used for test. In order to simulate real conditions in DNs, 10% 3rd and 5th harmonics are added to the signal, and the fundamental frequency is set to 50.2 Hz (the harmonic frequency is integer times of the fundamental one).

The results are shown in Table 6. As seen, when such a high-level noise condition is considered, the i-IpD^{2}FT can still meet M class requirements (in harmonic distortion conditions). The Maximum PE is 0.62 mrad, which is smaller than the limit of 0.87 mrad. Thus, we can conclude that the proposed method is suitable to be used in high-level noise condition.

4.6. Out-of-band Interferences

Interharmonics can be present in DNs because of the widely used time-varying loads (e.g., arc furnace). In the IEEE standard, an out-of-band interference test is also mandatorily required in the M class test.

In this test, the interharmonic frequency is varied [10, 25] or [75, 100) Hz in a step of 5 Hz. Unlike the IEEE standard, the interharmonic level is set to 4 values, which are 0.05%, 0.1%, 0.72%, 1%, 5%, and 10%, respectively. Please note that 0.1% and 0.72% are 2 thresholds used in the proposed method harmonic interharmonic detection. The fundamental frequency is varied in [47.5, 52.5] Hz with a step of 0.5 Hz. In Table 7, the corresponding results and limits are shown. As seen, the maximum FEs, RFEs, and PEs of the i-IpD^{2}FT are smaller than the corresponding limits, even though the interharmonic level is smaller than 10%. However, the IpD^{2}FT's errors are very large, and are out of the range that the IEEE standard requires. Also, when the interharmonic

Table 7. Maximum errors and corresponding limits in out-of-band interference test. SNR=80 dB

Parm.	**TVE (%)**	**FE (mHz)**	**RFE (Hz/s)**	**PE (mrad)**
Std.	1.3	10	–	0.87
i-IpD^{2}FT	0.09	9.26	0.84	0.46
IpD^{2}FT	4.60	505.75	82.96	45.62

Table 8. Results and corresponding limits in AM test. SNR=80 dB

Parm.	**TVE (%)**		**FE (mHz)**		**RFE (Hz/s)**		**PE (mrad)**	
Class	P	M	P	M	P	M	P	M
Std.	3	3	60	300	2.3	14	0.87	0.87
i-IpD^{2}FT	0.003	0.03	0.19	0.22	0.02	0.13	0.03	0.07
IpD^{2}FT	0.003	0.03	0.19	0.26	0.02	0.10	0.03	0.06

level is smaller than 0.1%, the results of the i-IpD^{2}FT can still meet the requirements. Thus, the threshold of 0.1% used for interharmonic detection is reasonable.

4.7. Modulations

In DNs, fundamental amplitude and phase (or frequency) can have modulations because of the unprecedented DERs and time-varying loads. It is necessary to test the i-IpD^{2}FT's performances under amplitude modulation (AM) and phase modulation (PM) conditions.

According to the IEEE standard, the amplitude modulation factor is 0.1, and the phase modulation factor is 0.1 rad. The maximum modulation frequency (both in AM and PM tests) is set to 2 Hz for the P class test and 5 Hz for the M class test. The maximum errors and the corresponding limits in the AM and PM tests are shown in Tables 8 and 9, respectively. Please note that the goal stated in section 1 is achieved with respect to AM and PM tests. The i-IpD^{2}FT has few errors in synchrophasor, ROCOF, and phase estimations. Compared with the AM test, the maximum FE in the PM test is much larger, which reaches 78.40 mHz in M class test. However, it is still much smaller than the FE limit, i.e., 300 mHz. Compared with the IpD^{2}FT, the i-IpD^{2}FT has larger estimation errors in PM test. This can be seen as the price for interharmonic interference suppression.

4.8. Frequency Ramps

In this section, we test the i-IpD^{2}FT's performances in the presence of frequency ramp. The ramp rate is set at ± 1 Hz/s. In the P class test, the fundamental frequency changes linearly from 48 Hz to 52 Hz (or opposite). By contrast, it changes linearly from 45 Hz to 55 Hz (or opposite) in the M class test.

Table 9. Results and corresponding limits in PM test. SNR=80 dB

Parm.	**TVE (%)**		**FE (mHz)**		**RFE (Hz/s)**		**PE (mrad)**	
Class	P	M	P	M	P	M	P	M
Std.	3	3	60	300	2.3	14	0.87	0.87
i-IpD^{2}FT	0.003	0.46	2.09	78.40	0.04	1.09	0.03	0.27
IpD^{2}FT	0.003	0.02	2.09	30.71	0.04	0.99	0.02	0.26

Table 10. Results and corresponding limits in frequency ramp test. SNR=80 dB

Parm.	**TVE (%)**		**FE (mHz)**		**RFE (Hz/s)**		**PE (mrad)**	
Class	P	M	P	M	P	M	P	M
Std.	1	1	10	10	0.4	0.2	0.87	0.87
i-IpD^{2}FT	0.002	0.003	0.13	0.18	0.01	0.02	0.02	0.02
IpD^{2}FT	0.002	0.003	0.14	0.19	0.01	0.02	0.02	0.02

The results and limits in the frequency ramp test are given in Table 10. Again, all the i-IpD^{2}FT's errors both in P and M class tests are much smaller than the corresponding limits. Particularly, the i-IpD^{2}FT's maximum PEs both in P and M class tests are only 0.02 mrad, which are much smaller than the limit stated in section 1, i.e., 0.87 mrad. The fundamental frequency pre-estimation and the Taylor signal model help us to achieve such high accuracy. It is interesting that the errors in P and M class tests are almost the same, except for the maximum FEs. This is because the i-IpD^{2}FT can pre-estimate the fundamental frequency based on the IpDFT. As a result, the impact of frequency deviation is negligible. Finally, in such a condition, the performances of the i-IpD^{2}FT and IpD^{2}FT are almost the same.

4.9. Step Changes

As stated in section 1, our goal is to propose a method to meet P and M class requirements simultaneously (i.e., high accuracy and fast response), and the PE should be smaller than 0.87 mrad. In sections 4.1-4.8, the accuracy tests are carried out, and it is verified that the i-IpD^{2}FT can meet the accuracy requirements. In this section, step change tests are carried out to test the i-IpD^{2}FT's responsiveness.

In the amplitude step change test, the fundamental amplitude is varied as 90% or 110% of the original value. Accordingly, $\pm\pi/18$ rad is added to the original fundamental phase in the phase step change test. The maximum response times and overshoots in amplitude and phase step change tests are shown in Tables 11 and 12, respectively. As seen, the maximum response times of the i-IpD^{2}FT, both in amplitude and phase step change tests, are much smaller than the P and M class limits. Thus, the i-IpD^{2}FT does have a fast response, and can meet the goal for fast response applications. Also, the maximum overshoots are always smaller than 5%, and are smaller than the corresponding limits. However, the maximum overshoots of the IpD^{2}FT are larger

Table 11. Response times, overshoots and corresponding limits in amplitude step change test. The overshoots are expressed in % of step magnitude. SNR=80 dB

Parm.	**TVE (ms)**		**FE (ms)**		**RFE (ms)**		**Overshoot (%)**	
Class	P	M	P	M	P	M	P	M
Std.	40	140	90	280	120	280	5	10
i-IpD^{2}FT	21.0	21.0	62.4	62.4	69.4	74.0	3.34	3.34
IpD^{2}FT	20.6	20.6	60.8	60.8	69.4	74.0	3.59	3.59

Table 12. Response times, overshoots and corresponding limits in phase step change test. The overshoots are expressed in % of step magnitude. SNR=80 dB

Parm.	**TVE (ms)**		**FE (ms)**		**RFE (ms)**		**Overshoot (%)**	
Class	P	M	P	M	P	M	P	M
Std.	40	140	90	280	120	280	5	10
i-IpD^{2}FT	25.3	25.3	70.0	70.0	74.0	76.3	4.70	4.70
IpD^{2}FT	24.6	24.6	67.5	67.5	74.0	76.3	5.04	5.04

than 5% (the P class limit), which means the Kaiser window used in the i-IpD^{2}FT is reasonable. The delay times, both in amplitude and phase step change tests, are always smaller than 2 ms, which is much smaller than the limit of 5 ms (both for P and M class tests).

5. Conclusion

In this paper, we propose a novel synchrophasor estimator, especially for DN applications. The optimal DTFT frequency selection and TFM-based method are used to suppress both low- and high-level interharmonics. The Kaiser-based IpD^{2}FT is used in transient conditions to meet response time requirements. All the threshold are obtained over numerous simulations, which makes the proposed method robust to various disturbances.

Simulation tests show that the i-IpD^{2}FT can have high accuracy in synchrophasor, frequency, ROCOF, and phase estimations, both in canonical and peculiar tests. Particularly, the maximum PEs in all accuracy tests are always smaller than 0.87 mrad. Meanwhile, the i-IpD^{2}FT can also meet P class response time requirements, and thus have a fast response in transient conditions. The computation time of the i-IpD^{2}FT is much smaller than 20 ms, and can meet the requirement of high reporting rate PMUs, i.e., RR =50 frames/s. The reporting latency is smaller than 40 ms, which can meet the P class latency requirement. In conclusion, such excellent performances verify that the i-IpD^{2}FT can be used in D-PMUs.

References

[1] Petri D, Fontanelli D and Macii D 2014 *IEEE Trans. Instrum. Meas.* **63** 2330–2340 ISSN 0018-9456

[2] IEEE 2011 *IEEE Standard for Synchrophasor Measurements for Power Systems* (IEEE Std C37.118.1-2011 (Revision of IEEE Std C37.118-2005))

[3] IEEE 2014 *IEEE Standard for Synchrophasor Measurements for Power Systems – Amendment 1: Modification of Selected Performance Requirements* (IEEE Std C37.118.1a-2014 (Amendment to IEEE Std C37.118.1-2011))

[4] Chen L, Zhao W, Yu Y, Wang Q and Huang S 2018 Improved interpolated dynamic DFT synchrophasor estimator considering second harmonic interferences *Proc. IEEE Int. Instrum. Meas. Technol. Conf. (I2MTC)* pp 1–6

[5] Chen L, Zhao W, Wang F, Wang Q and Huang S 2018 *Sensors* **18** 2748

[6] Roscoe A J 2013 *IEEE Trans. Instrum. Meas.* **62** 2140–2153 ISSN 0018-9456

[7] Castello P, Liu J, Muscas C, Pegoraro P A, Ponci F and Monti A 2014 *IEEE Trans. Instrum. Meas.* **63** 2837–2845 ISSN 0018-9456

[8] Derviskadic A, Romano P and Paolone M 2018 *IEEE Trans. Instrum. Meas.* **67** 547–558 ISSN 0018-9456

[9] Belega D and Petri D 2013 *IEEE Trans. Instrum. Meas.* **62** 942–953

[10] de la O Serna J A 2007 *IEEE Trans. Instrum. Meas.* **56** 1648–1657 ISSN 0018-9456

[11] a J Platas-Garza M A P and de la O Serna J A 2010 *IEEE Trans. Instrum. Meas.* **59** 1803–1811 ISSN 0018-9456

[12] Bertocco M, Frigo G, Narduzzi C, Muscas C and Pegoraro P A 2015 *IEEE Trans. Instrum. Meas.* **64** 3274–3283

[13] Bertocco M, Frigo G, Giorgi G and Narduzzi C 2015 Frequency tracking for efficient phasor measurement based on a CSTFM model *Proc. IEEE Int. Work. Appl. Meas. Power Syst. (AMPS)* pp 84–89

[14] Frigo G, Giorgi G, Bertocco M and Narduzzi C 2016 Multifunction phasor analysis for distribution networks *Proc. IEEE Int. Work. Appl. Meas. Power Syst. (AMPS)* pp 1–6

[15] Frigo G, Giorgi G and Narduzzi C 2016 Efficient detection for multifrequency dynamic phasor analysis *Proc. IEEE Int. Work. Appl. Meas. Power Syst. (AMPS)* pp 1–6

[16] Xia T and Liu Y 2010 *IEEE Trans. Power Syst.* **25** 844–852 ISSN 0885-8950

[17] Zhan L, Liu Y and Liu Y 2018 *IEEE Trans. Smart Grid* **9** 67–77 ISSN 1949-3053

[18] Zhan L, Liu Y, Culliss J, Zhao J and Liu Y 2015 *IEEE Trans. Smart Grid* **6** 2013–2022 ISSN 1949-3053

[19] Barchi G, Fontanelli D, Macii D and Petri D 2015 *IEEE Trans. Instrum. Meas.* **64** 1129–1139 ISSN 0018-9456

[20] 50160 E 2010 *Voltage Characteristics of Electricity Supplied by Public Electricity Networks,* (EN 50160)

[21] Frigo G, Derviskadic A and Paolone M 2018 *IEEE Trans. Instrum. Meas.* 1–16 ISSN 0018-9456

[22] Agrez D 2002 *IEEE Trans. Instrum. Meas.* **51** 287–292 ISSN 0018-9456

[23] Chen L, Zhao W, Wang F, Wang Q and Huang S 2019 *IEEE Trans. Instrum. Meas.* **68** 1714–1723 ISSN 0018-9456

[24] Macii D, Petri D and Zorat A 2012 *IEEE Trans. Instrum. Meas.* **61** 2653–2664

[25] Bertocco M, Frigo G, Narduzzi C, Muscas C and Pegoraro P A 2015 *IEEE Trans. Instrum. Meas.* **64** 3274–3283 ISSN 0018-9456

[26] Castello P, Ferrero R, Pegoraro P A and Toscani S 2018 *IEEE Trans. Instrum. Meas.* **67** 1036–1046 ISSN 0018-9456